IEEE Photonics Journal
An IEEE Photonics Society Publication

Invited Paper

Towards a Practical Implementation of Coherent WDM: Analytical, Numerical, and Experimental Studies

Volume 2, Number 5, October 2010

S. K. Ibrahim, Member, IEEE
J. Zhao, Member, IEEE
F. C. Garcia Gunning, Member, IEEE
P. Frascella, Student Member, IEEE
F. H. Peters
A. D. Ellis

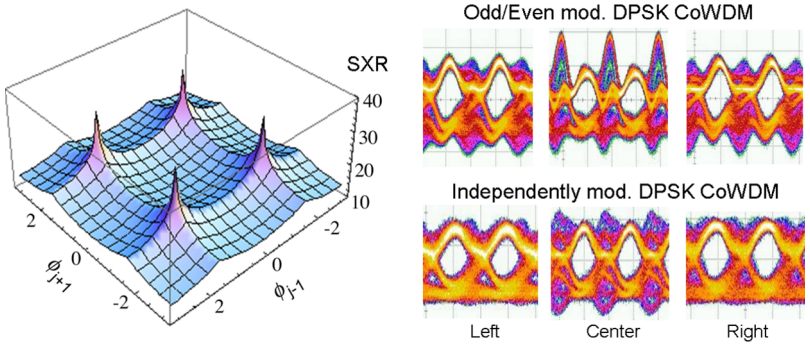

DOI: 10.1109/JPHOT.2010.2071859
1943-0655/$26.00 ©2010 IEEE

Towards a Practical Implementation of Coherent WDM: Analytical, Numerical, and Experimental Studies

S. K. Ibrahim, *Member, IEEE*, J. Zhao, *Member, IEEE*, F. C. Garcia Gunning, *Member, IEEE*, P. Frascella, *Student Member, IEEE*, F. H. Peters, and A. D. Ellis

(Invited Paper)

Department of Physics and Tyndall National Institute, University College Cork, Cork, Ireland

DOI: 10.1109/JPHOT.2010.2071859
1943-0655/$26.00 ©2010 IEEE

Manuscript received July 19, 2010; revised August 21, 2010; accepted August 21, 2010. Date of publication August 28, 2010; date of current version September 17, 2010. This material is based upon work supported by Science Foundation Ireland under Grant 06/IN/I969 and Grant 03/CE3/I405 and from the European Communities Seventh Framework Program FP/2007-2013 under Grant agreement 224547 (PHASORS). Corresponding author: S. K. Ibrahim (e-mail: selwan.ibrahim@tyndall.ie).

Abstract: Future optical networks will require the implementation of very high capacity (and therefore spectral efficient) technologies. Multi-carrier systems, such as Orthogonal Frequency Division Multiplexing (OFDM) and Coherent WDM (CoWDM), are promising candidates. In this paper, we present analytical, numerical, and experimental investigations of the impact of the relative phases between optical subcarriers of CoWDM systems, as well as the effect that the number of independently modulated subcarriers can have on the performance. We numerically demonstrate a five-subcarrier and three-subcarrier 10-GBd CoWDM system with direct detected amplitude shift keying (ASK) and differentially/coherently detected (D) phase shift keying (PSK). The simulation results are compared with experimental measurements of a 32-Gbit/s DPSK CoWDM system in two configurations. The first configuration was a practical 3-modulator array where all three subcarriers were independently modulated, the second configuration being a traditional 2-modulator odd/even configuration, where only odd and even subcarriers were independently modulated. Simulation and experimental results both indicate that the independent modulation implementation has a greater dependency on the relative phases between subcarriers, with a stronger penalty for the center subcarrier than the odd/even modulation scheme.

Index Terms: Optical fiber communication, optical modulation, phase modulation.

1. Introduction

The rapid growth in video-based Internet applications is driving the demand for higher speed optical transmission systems for the access, metro-core, and long-haul networks, which requires bandwidth efficient telecommunications systems. One promising approach is the use of optical multi-carrier spectrally efficient transmission techniques, where the subcarrier spacing is equal to its symbol rate [1]–[20]. This was demonstrated by optically generated Orthogonal Frequency Division Multiplexing (all-optical OFDM) [2]–[8], optically generated Coherent Wavelength Division Multiplexing (CoWDM) [9]–[13], and traditional electrically generated OFDM [14], [15], as well as combining all-optical and traditional electrical OFDM techniques resulting in multi-banded, electro-optical OFDM [16]–[19]. All-optical implementations of OFDM/CoWDM offer the prospect of high

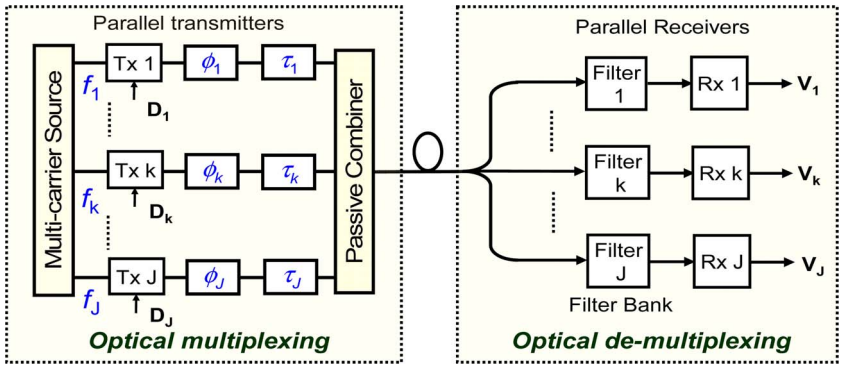

Fig. 1. General schematic of a CoWDM system.

aggregate capacity and spectral efficiency, with impairment tolerances scaling with the symbol rate of each subcarrier. However, the majority of earlier reports of such techniques tended to use only two modulators in an odd/even configuration. This configuration does not address the practical implementation penalties arising from the fact that neighboring subcarriers carry different data patterns with overlapping spectra [11]–[13].

Typically, in all-optical OFDM systems, unless ideal matched filters are deployed [7], [8], non-ideal filters result in residual inter-channel crosstalk at the receiver-side, whose influence on system performance is related to the relative phases between the subcarriers. This impact can be mitigated by increasing the guard band interval [6], reducing the number of interfering channels through polarization interleaving [3] or by using lower number of subcarriers [4], restoring the channel orthogonality at the transmitter through electronic pre-compensation [20], [21], or via phase control for each subcarrier, resulting in the reduction of signal-crosstalk beating at the decision point (CoWDM) [9]–[13]. CoWDM also offers the advantage of using low-cost receiver filters without the need for expensive and power-hungry DSP-based receivers.

In this paper, we examine the use of phase control in the transmitter to control the crosstalk arising from the neighbor interfering optical subcarriers due to the partially overlapping spectra with the targeted subcarrier at the transmitter. It is important to study this effect because, in practical realizations, the phase between the subcarriers may vary due to any random environment changes, such as temperature, that would cause random length changes resulting in random phase variations. We present, for the first time, an analytical theory of the residual crosstalk penalty, which is verified by direct numerical simulations of CoWDM with Amplitude Shift Keying (ASK), Differential Phase Shift Keying (DPSK), and Binary Phase Shift Keying (BPSK) modulation formats. Moreover, we experimentally verify the predicted impact of the nearest-neighbor crosstalk in a 3-subcarrier 32-Gbit/s DPSK CoWDM system.

The paper is organized as follows. In Section 2, we present an analytical theory of the phase relationship between subcarriers on CoWDM systems. This analysis is further investigated by numerical simulations in Section 3, which demonstrate a 5-subcarrier and 3-subcarrier 10-GBd CoWDM system with direct detected ASK, and differentially (coherently) detected DPSK (BPSK) to illustrate the phase and filter bandwidth effects on the performance of these systems. In Section 4, the theory and numerical simulations are confirmed by direct experimental observations for a 3-subcarrier 32 Gbit/s DPSK CoWDM system using a 3-modulator independently modulated array configuration consisting of three independently modulated subcarriers and an odd/even modulated configuration using only two modulators instead. Finally, Section 5 will conclude the paper.

2. Analytical Theory

Fig. 1 shows a general schematic of a multi-carrier CoWDM system where the subcarriers are optically multiplexed at the transmitter side (left) and optically demultiplexed and demodulated at the receiver side (right).

In order to analyze the optical field $E_k^0(t)$ of any k WDM channel with a symbol period T and field amplitude E_0, we assume a complex logical data for the nth bit of the kth channel $(D_{k,n})$, a pulse shape $h_{Tx}(t)$ with relative delay τ_k, and an optical carrier with frequency ω_k and phase ϕ_k:

$$E_k^0(t) = \sum_{n=-\infty}^{+\infty} D_{k,n} E_0 h_{Tx}(t - \tau_k - nT) e^{i(\omega_k t + \phi_k)}. \tag{1}$$

Note that $h_{Tx}(t)$ represents the optical pulse shape after modulation, and thus, it is the overall system response at the transmitter including pulse shape of the logic data, impulse response of the electrical filter, transfer function of modulation, and the impulse response of any optical filter deployed within the transmitter. In practice, $h_{Tx}(t)$ is usually the same for all subcarriers. Assuming that the targeted subcarrier j is optically demultiplexed using a receiver-side filter with a frequency response $H_{Rx,j}(\omega)$, the spectrum of the optical field after filtering can be represented as

$$\varepsilon_j'(\omega) = \sum_{k=1}^{J} \sum_{n=-\infty}^{+\infty} D_{k,n} E_0 e^{i\phi_k} H_{Tx}(\omega - \omega_k) e^{-i(\tau_k + nT)(\omega - \omega_k)} H_{Rx,j}(\omega) \tag{2}$$

where J is the number of subcarriers, and $H_{Tx}(\omega)$ is the equivalent frequency response corresponding to the transmitter impulse response $h_{Tx}(t)$. The time-domain signal after channel demultiplexing for the subcarrier j is obtained by taking the inverse Fourier transform of (2)

$$E_j'(t) = E_0 \sum_{k=1}^{J} \sum_{n=-\infty}^{\infty} S_{k,n} I_{k,j}(t - \tau_k - nT) e^{i\omega_j t + i(\omega_k - \omega_j)(nT + \tau_k)} \tag{3}$$

where $S_{k,n} = D_{k,n} e^{i\phi_k}$ represents the complex logical data, including the subcarrier phase, and

$$I_{k,j}(t) = \frac{1}{2\pi} \int_{-\infty}^{+\infty} H_{Tx}(\omega - \omega_k + \omega_j) H_{Rx,j}(\omega + \omega_j) e^{i\omega t} d\omega \tag{4}$$

is the baseband representation of the signal pulse shape for the kth channel after optical filtering by the demultiplexing filter targeted to the subcarrier j.

For an orthogonal multi-carrier system, we assume that all subcarriers are temporally aligned with a zero delay, i.e., $\tau_k = 0$, and that the channel spacing satisfies the orthogonality condition $\omega_k - \omega_j = 2\pi \cdot r/T$, where r is an integer. Note that, unless the carrier phase ϕ_k is constant, the orthogonality condition is only approximately satisfied, since any time variation in phase may also be expressed as a change in carrier frequency.

In order to determine the detected electrical signal $V_j(t)$, one must first identify the detection method. In direct-detected systems $V_j(t)$ is given by

$$V_j(t) \propto \left| E_0 \sum_{k=1}^{J} \sum_{n=-\infty}^{\infty} S_{k,n} I_{k,j}(t - nT) \right|^2. \tag{5}$$

While in the homodyne coherent-detected system, i.e., when $\omega_{lo} = \omega_j$, $V_j(t)$ is then given by

$$\begin{matrix} V_{j,in-phase}(t) \\ V_{j,quadrature}(t) \end{matrix} \propto \begin{matrix} \mathrm{Re} \\ \mathrm{Im} \end{matrix} \left\{ E_0 \sum_{k=1}^{J} \sum_{n=-\infty}^{\infty} S_{k,n} I_{k,j}(t - nT) e^{-i\phi_{lo}} \right\} \tag{6}$$

where $I_{k,j}(t)$ should be interpreted in a more generic form, taking into consideration the effect of receiver-side electrical filter, which may also be implemented digitally [5], [16]:

$$I_{k,j}(t) = \frac{1}{2\pi} \int_{-\infty}^{+\infty} H_{Tx}\left(\omega - \frac{2\pi r}{T}\right) H_{Rx,j}(\omega + \omega_j) H_{ele,j}(\omega) e^{i\omega t} d\omega. \tag{7}$$

We may observe from (3) that if $I_{k,j}(t) = 0$ at the sampling instant for any $k \neq j$, the system is crosstalk free. Possible conditions for crosstalk free operation (i.e., using matched filters at the receiver) may include a receiver filter with a $sinc(\omega T/2)$ frequency profile coupled with ideal rectangular temporal pulses from the transmitter [1] or a receiver filter with rectangular frequency responses coupled with transmitted pulse trains with rectangular spectra [21]. Low crosstalk has also been observed using practical bandwidth limited transmitters and filters by performing optical Fourier transform at the receiver [7], [8].

2.1. Direct Detection for ASK Signals

In the case of direct detection for ASK signals, (5) may be expanded in order to give terms related to the targeted signal level, intersymbol interference, and crosstalk, when the sampling instant for the mth sample is mT:

$$V_j(mT) \propto \left(D_{j,m} I_{j,j}(0) e^{i\phi_j} + \sum_{n \neq m} D_{j,n} I_{j,j}((m-n)T) e^{i\phi_j} + \sum_{k \neq j} \sum_{n} D_{k,n} I_{k,j}((m-n)T) e^{i\phi_k} \right) \cdot \left(D^*_{j,m} I^*_{j,j}(0) e^{-i\phi_j} + \sum_{q \neq m} D^*_{j,q} I^*_{j,j}((m-q)T) e^{-i\phi_j} + \sum_{p \neq j} \sum_{q} D^*_{p,q} I^*_{p,j}((m-q)T) e^{-i\phi_k} \right). \quad (8)$$

By making a reasonable assumption that the crosstalk is dominated by the nearest neighbor subcarriers, i.e., $D_{j,m}$ is only degraded by $D_{j-1,m}$ and $D_{j+1,m}$, and, for simplicity, neglecting intersymbol interference, one can expand the multiplication in (8), giving

$$\begin{aligned} V_j(mT) \propto & \left|D_{j,m} I_{j,j}(0)\right|^2 + \left|D_{j-1,m} \cdot I_{j-1,j}(0)\right|^2 + \left|D_{j+1,m} \cdot I_{j+1,j}(0)\right|^2 \\ & + 2 D_{j,m} D_{j-1,m} \cdot I_{j-1,j}(0) I_{j,j}(0) \cdot Cos(\phi_j - \phi_{j-1}) \\ & + 2 D_{j,m} D_{j+1,m} \cdot I_{j+1,j}(0) I_{j,j}(0) \cdot Cos(\phi_j - \phi_{j+1}) \\ & + 2 D_{j-1,m} D_{j+1,m} \cdot I_{j-1,j}(0) I_{j+1,j}(0) \cdot Cos(\phi_{j-1} - \phi_{j+1}). \end{aligned} \quad (9)$$

Here, it was also assumed that the data sequences are in a single quadrature and, without loss of generality, are along the real axis.

Finally, we define a signal to crosstalk ratio (SXR) as the minimum difference between the signal levels "0" and "1" in the absence of crosstalk, divided by the sum of the maximum crosstalk levels on "1" and "0," taking the worst-case data pattern of the adjacent subcarriers. Here, it becomes

$$SXR = \min|_{D_{k,n}} \left(\frac{\text{intensity for '1'} - \text{intensity for '0'}}{|\text{Crosstalk in '1' level}| + |\text{Crosstalk in '0' level}|} \right). \quad (10)$$

The value of SXR and the associated worst-case data pattern of the adjacent subcarriers depend on the phases of the adjacent subcarrier. However, for the arbitrary phase, we can obtain a lower bound for the SXR:

$$\text{Min}(SXR_{dd}) = \frac{|I_{j,j}(0)|^2}{2|I_{j-1,j}(0)|^2 + 2|I_{j+1,j}(0)|^2 + 2|I_{j-1,j}(0) I_{j,j}(0) \cos(\phi_j - \phi_{j-1})| + 2|I_{j+1,j}(0) I_{j,j}(0) \cos(\phi_j - \phi_{j+1})| + 4|I_{j-1,j}(0) I_{j+1,j}(0) \cos(\phi_{j-1} - \phi_{j+1})|}. \quad (11)$$

If the phases of CoWDM subcarriers are controlled to be $\phi_j = \phi_0 + j\pi/2$, the signal-crosstalk beating terms can be eliminated, regardless of the logic data of the $(j-1)$th, jth, and $(j+1)$th carrriers. Consequently, the sampled value is determined only by the signal level and the crosstalk-crosstalk

beating. That is, the interference signal between the two nearest neighbors resulting in the SXR value low-bounded by

$$\text{Min}(SXR_{dd})|_{\phi_j=\phi_0+j\pi/2}=\frac{\left|I_{j,j}(0)\right|^2}{2\left|I_{j-1,j}(0)\right|^2+2\left|I_{j+1,j}(0)\right|^2+4\left|I_{j-1,j}(0).I_{j+1,j}(0)\right|}. \tag{12}$$

If further assumption is made that the neighboring subcarriers $(j-1)$ and $(j+1)$ carry the same data logic i.e., $D_{j-1,m}=D_{j+1,m}$, and $I_{j-1,j}(0)=I_{j+1,j}(0)$, the crosstalk terms in (9) can be fully eliminated at an appropriate phase. This case occurs for multi-carrier configurations using two modulators for odd/even subcarrier modulation.

2.2. Differential Direct Detection for BPSK Signals

If differential detection is assumed for DPSK signals, the received electrical signals from the constructive $(+)$ and destructive $(-)$ paths can be given by

$$V_j^{\pm}(t)\propto\left|\sum_{k=1}^{J}\sum_{n=-\infty}^{\infty}\left(S_{k,n}I_{k,j}(t-nT)e^{i\omega_j t+i\left(\frac{2\pi r}{T}\right)(nT)}\pm S_{k,n}I_{k,j}(t-(n-1)T)e^{i\omega_j(t+T)+i\left(\frac{2\pi r}{T}\right)(nT)}\right)\right|^2. \tag{13}$$

Therefore, the sampled value for the mth bit is

$$V_j^{\pm}(mT)\propto\left|\sum_{k=1}^{J}\sum_{n=-\infty}^{\infty}(D_{k,n}+D_{k,n+1}e^{+i\omega_j T})I_{k,j}(t-nT)e^{i\omega_j t+i\phi_k}\right|^2. \tag{14}$$

In order to facilitate the derivation, we define new variables representing the decoded data from the constructive and destructive paths in terms of the transmitted (pre-coded) symbols

$$D_{k,n}^{\pm}=D_{k,n}\pm D_{k,n+1}e^{i\omega_k T}. \tag{15}$$

Similar to direct detection, $I_{j,j}(t)$, which is the pulse shape of the jth subcarrier after its optical bandpass filtering (OBPF) (before demodulation), is assumed to be intersymbol interference (ISI) free. It is also assumed that the crosstalk of the jth subcarrier is generated by the nearest neighbors $(k=j\pm1)$. Therefore, one can derive $V_j^{\pm}$ as

$$\begin{aligned}V_j^{\pm}(mT)\propto\Bigg(&\left|D_{j,m}^{\pm}I_{j,j}(0)\right|^2+\left|D_{j-1,m}^{\pm}\cdot I_{j-1,j}(0)\right|^2+\left|D_{j+1,m}^{\pm}\cdot I_{j+1,j}(0)\right|^2\\&+2\text{Re}\left\{D_{j,m}^{\pm}\cdot D_{j-1,m}^{\pm^*}e^{i(\phi_j-\phi_{j-1})}\right\}\cdot I_{j-1,j}(0)I_{j,j}(0)\\&+2\text{Re}\left\{D_{j,m}^{\pm}\cdot D_{j+1,m}^{\pm^*}e^{i(\phi_j-\phi_{j+1})}\right\}\cdot I_{j+1,j}(0)I_{j,j}(0)\\&+2\text{Re}\left\{D_{j-1,m}^{\pm}\cdot D_{j+1,m}^{\pm^*}e^{i(\phi_{j-1}-\phi_{j+1})}\right\}\cdot I_{j-1,j}(0)I_{j+1,j}(0).\end{aligned} \tag{16}$$

When calculating the correspondent SXR, it can be observed that, in DPSK, the SXR for the arbitrary phase of a single-ended differential detection is low bounded by

$$\text{Min}(SXR_{diff})=\frac{\left|I_{j,j}(0)\right|^2}{\left|I_{j-1,j}(0)\right|^2+\left|I_{j+1,j}(0)\right|^2+2\left|I_{j-1,j}(0)I_{j,j}(0)\cos(\phi_j-\phi_{j-1})\right|+2\left|I_{j+1,j}(0)I_{j,j}(0)\cos(\phi_j-\phi_{j+1})\right|+2\left|I_{j-1,j}(0)I_{j+1,j}(0)\cos(\phi_{j-1}-\phi_{j+1})\right|}. \tag{17}$$

In the case of $\phi_j = \phi_0 + j\pi/2$, similar to direct detection, the signal-crosstalk beating terms are eliminated, and therefore, the low bounded SXR can be obtained from

$$\begin{aligned}\text{Min}(SXR_{diff})|_{\phi_j=\phi_0+j\pi/2} &= \frac{|I_{j,j}(0)|^2}{|I_{j-1,j}(0)|^2+|I_{j+1,j}(0)|^2+2|I_{j+1,j}(0).I_{j-1,j}(0)|} \\ &= 2\times \text{Min}(SXR_{dd})|_{\phi_j=\phi_0+j\pi/2}. \end{aligned} \quad (18)$$

In the CoWDM odd/even modulated configuration using only two modulators, i.e., $D_{j-1,m} = D_{j+1,m}$, the crosstalk terms in (16) can also be fully eliminated, which will be demonstrated numerically and experimentally in the next sections.

2.3. Coherent Detection

In this case, for simplicity, the polarization of the input CoWDM is assumed to be controlled to match that of the local oscillator. Assuming the use of a 90° optical hybrid with balanced photodiodes for the jth channel, the sampled value for the in-phase and quadrature components for the mth bit is given by

$$\begin{aligned}\begin{matrix}V_{j,in-phase}(mT)\\ V_{j,quadrature}(mT)\end{matrix} \propto \begin{matrix}\text{Re}\\ \text{Im}\end{matrix}\Bigg\{ & D_{j,m}I_{j,j}(0)e^{i\phi_j - i\phi_{lo}} + \sum_{n\neq m} D_{j,n}I_{j,j}((m-n)T)e^{i\phi_j - i\phi_{lo}} \\ & + \sum_{k\neq j}\sum_{n} D_{k,n}I_{k,j}((m-n)T)e^{i\phi_k - i\phi_{lo}}\Bigg\}. \end{aligned} \quad (19)$$

Again, the ISI is neglected, and it is assumed that the crosstalk comes only from the adjacent subcarriers $D_{j-1,m}$ and $D_{j+1,m}$:

$$\begin{aligned}\begin{matrix}V_{j,in-phase}(mT)\\ V_{j,quadrature}(mT)\end{matrix} \propto \begin{matrix}\text{Re}\\ \text{Im}\end{matrix}\Big\{ & D_{j,m}I_{j,j}(0)e^{i\phi_j - i\phi_{lo}} + D_{j-1,m}I_{j-1,j}(0)e^{i\phi_{j-1} - i\phi_{lo}} \\ & + D_{j+1,m}I_{j+1,j}(0)e^{i\phi_{j+1} - i\phi_{lo}}\Big\}. \end{aligned} \quad (20)$$

In back-to-back PSK, or any other single quadrature modulation format, $D_{k,n}$ and $I_{k,n}(t)$ may be considered to be real. Therefore, the in-phase component can be expressed as

$$\begin{aligned}V_{j,in-phase}(mT) \propto & D_{j,m}I_{j,j}(0)\cos(\phi_j - \phi_{lo}) + D_{j-1,m}I_{j-1,j}(0)\cos(\phi_{j-1} - \phi_{lo}) \\ & + D_{j+1,m}I_{j+1,j}(0)\cos(\phi_{j+1} - \phi_{lo}) \end{aligned} \quad (21)$$

and the quadrature component is the same, except for the cos() terms, which are replaced with sin().

Therefore, the low bounded SXR is

$$\text{Min}(SXR_{CD}) = \frac{|I_{j,j}(0)|}{|I_{j-1,j}(0)\cos(\phi_j - \phi_{j-1})| + |I_{j+1,j}(0)\cos(\phi_j - \phi_{j+1})|}. \quad (22)$$

In the case of $\phi_j = \phi_0 + j\pi/2$ and for a single quadrature signal, (20) shows that the crosstalk is orthogonal to the signal field and, consequently, results in an infinite SXR. The impact of the crosstalk is shown in Fig. 2 for two particular phase relationships between the subcarriers: $\phi_j = \phi_0 + j\pi/2$ and $\phi_j = \phi_0$. The length of the blue arrows represents the crosstalk level, which is determined by the filter responses $I_{k,j}(0)$, while the position along the blue arrow is determined by the data carried by the interfering subcarriers. Clearly, when $\phi_j = \phi_0 + j\pi/2$, it is possible to arrange

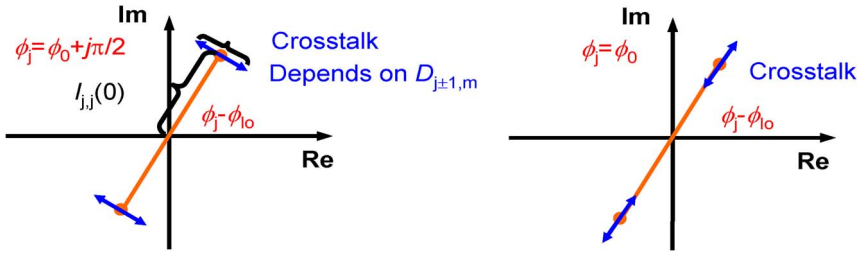

Fig. 2. Constellation map of PSK with crosstalk with different subcarrier phase relationships.

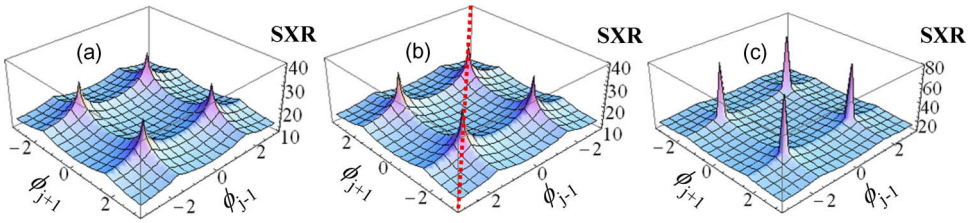

Fig. 3. Variation in the SXR as a function of the relative phase of the two nearest-neighbor sub-channels for (a) direct detected ASK signal, (b) differentially detected BPSK signal, and (c) coherent detected BPSK signal with the filter performance characterized by $I_{j\pm1,j}(0) = 0.01 \times I_{j,j}(0)$ (the dotted red line shows the projection for the phase relationship $(\phi_{j-1} = 0, \phi_j, \phi_{j+1} = 0)$).

for the crosstalk to fall orthogonally to the signal, consequently eliminating any impact from the crosstalk.

In general, a summary of the derivations from Sections 2.1–2.3 is represented in Fig. 3. It shows that the variation in the SXR for systems where the crosstalk amplitude of the nearest neighbors, at the sampling instant of the targeted channel j, is 1% of the signal level on that sample $I_{j\pm1,j}(0) = 0.01 \times I_{j,j}(0)$ and that the filters are chirp free.

The figure clearly shows that the SXR is optimal when the phase difference between adjacent sub-channels is $\pi/2$ for all cases. Furthermore, under optimized phase, coherent detection results in a higher SXR, indicating its advantages when compared with other detection methods. However, this simple analytical treatment suggests that if residual crosstalk exists $(I_{kj}(mT) \neq 0)$, the number of independent modulated signals has a significant impact on the results.

3. Numerical Simulations

3.1. Simulations for a Five-Subcarrier CoWDM System

In Section 2, we assumed, for clarity, that the filters were ISI free. However, this is unlikely to be the case for the $(j + 1)$th channel passing through the jth filter. Numerical simulations were performed in to verify the general trends of the analytical approach and to examine the impact of ISI.

Fig. 4 shows the simulation model of the CoWDM system used in this paper. The first stage of the CoWDM system is the comb generator/laser source which is used to generate the equally spaced sub-carriers at a frequency equal to the symbol rate of a single channel. In this case, five coherent optical subcarriers with equal intensities and phases were produced using a comb generator. The subcarrier spacing was 10 GHz, which is equal to the data rate of each subcarrier, which were modulated by uncorrelated 10-Gbit/s data streams with temporally aligned eye crossings for ASK, DPSK, and BPSK modulation formats. The data streams consisted of $2^{11} - 1$ pseudo-random binary sequences (PRBS) repeated five times (10, 235 bits) and delayed by 6, 70, 101, 125 and 205 bits in order to obtain the uncorrelated bit sequences. Ten "0" bits and 11 "0" bits were added before and after each data train to simplify the boundary conditions. The electrical "1" bits were raised-cosine shaped with a roll-off coefficient of 0.4 and were simulated with 40 samples per bit.

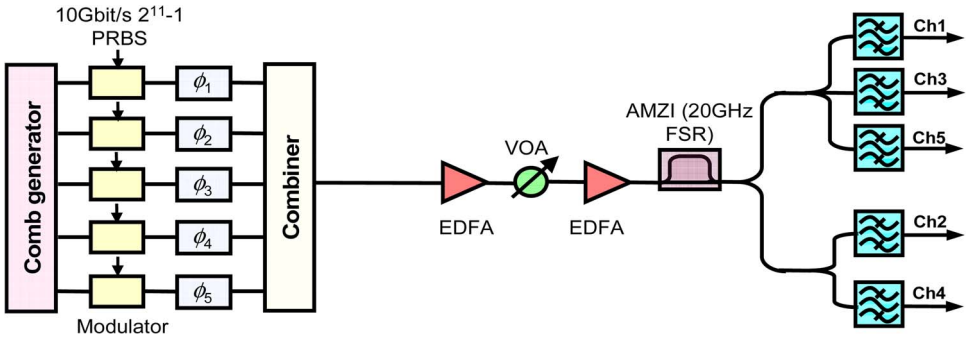

Fig. 4. Simulation setup of a five-subcarrier CoWDM system.

The modulated subcarriers were phase shifted by $k \times \Delta\phi$ $(k = 0, \ldots, 4)$ before they were passively combined. Note that, although only one variable $\Delta\phi$ was used to investigate the influence of phase difference between subcarriers, these phase shifts are expected to include the best and the worst performance cases, as illustrated in Fig. 3.

At the receiver, the noise of the optical preamplifier was modeled as additive white Gaussian noise with equal noise spectral power density for each polarization. We followed the conventional CoWDM demultiplexing approach [9]–[13], which may also be viewed as a one tap-discrete Fourier transform (DFT) filter [2], [6], [7] in which the five subcarriers were demultiplexed by an asymmetric Mach–Zehnder interferometer (AMZI), with 20 GHz free spectral range (FSR) to separate the odd and even subcarriers, followed by third-order Gaussian-shaped optical bandpass filters (OBPFs). The signals after the OBPFs had a power of -3 dBm per subcarrier and were detected directly (ASK), differentially (DPSK), or coherently (BPSK) using balanced detection. In coherent detection, the signals and local oscillators were separated into two linear polarization components with polarization beam splitters (PBSs), mixed by 90° optical hybrids, and detected by balanced detectors to extract the in-phase and quadrature components. The output powers of the local oscillators were $+10$ dBm, and their phases were assumed not to vary during the simulation, and therefore, electrical phase equalization was not required. The equivalent thermal noise spectral power density of the detectors was 18 pA$/\sqrt{}$Hz. After optical-to-electrical conversion, the signals were electrically amplified, filtered by a 15-GHz fourth-order Bessel electrical filters (EFs), sampled, and decoded by optimal threshold decoding. The simulation was iterated 10 times with different random number seeds to give a total of 102 350 simulated bits. The performance was evaluated in terms of the required normalized optical signal-to-noise ratio (OSNR) at the photodiode to achieve a bit error rate (BER) of 5×10^{-4} by direct error counting. The simulated bit number produces a confidence interval of $[3 \times 10^{-4} - 7.5 \times 10^{-4}]$ for this BER with 99% certainty. The normalized OSNR was defined by

$$\textit{Normalized OSNR} = \frac{\textit{Total Signal Power}}{5 \times \textit{Noise Power in } 0.1 \text{ nm}}. \tag{23}$$

Fig. 5 shows the performance of the center (Ch3—squares), inner (Ch2/Ch4—triangles), and outer subcarriers (Ch1/Ch5—circles) against the bandwidth of the OBPF for (a) ASK, (b) DPSK, and (c) BPSK, with a phase difference between subcarriers of $\pi/2$. It is clear from the figure that the optimized filter bandwidths lie between 1.5 and 2.5$\times$ the baud rate (15–25 GHz) for all cases. The OBPF bandwidth should be selected to achieve not only a balance between inter-symbol interference and inter subcarrier crosstalk but also a balance between the crosstalk from the most adjacent subcarrier, referred to herein as inner-neighbors, and that from the next nearest subcarriers (or outer-neighbors). At the narrower bandwidth region ($<$ 15 GHz), the crosstalk from the inner-neighbors dominated. Consequently, Ch1/Ch5, which only had one inner-neighbor, exhibited better performance than Ch2/Ch4 and Ch3, having two inner-neighbors. However, at the

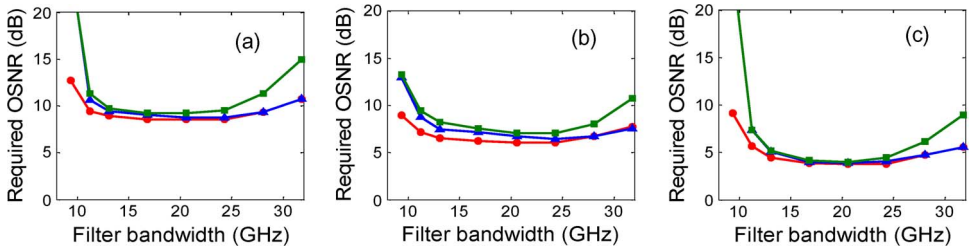

Fig. 5. Performance of Ch1-5 versus the bandwidth of the OBPF for (a) ASK, (b) DPSK, and (c) BPSK modulation formats (Ch1/Ch5: red circles; Ch2/Ch4: blue triangles; Ch3: green squares).

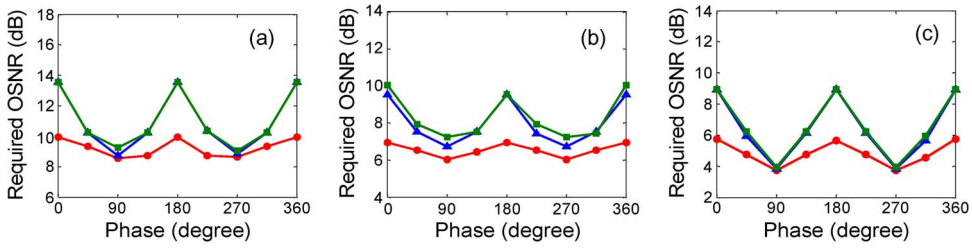

Fig. 6. Normalized OSNR versus the phase $\Delta\phi$ for Ch1-5 when the modulation format is (a) ASK, (b) DPSK, and (c) BPSK (Ch1/Ch5: red circles; Ch2/Ch4: blue triangles; Ch3: green squares).

wider bandwidth region (> 25 GHz), the crosstalk levels for the subcarriers with two outer neighbors increased significantly. Furthermore, at the optimum phase $\phi_j = \phi_0 + j\pi/2$, the influence of the inner neighbors was mitigated such that the crosstalk from the outer neighbors dominated the system performance. Consequently, Ch2/Ch4 had similar performance as Ch1/Ch5 because they only had one outer neighbor, and all were better than that of Ch3, which had two outer neighbors.

In Fig. 6, the phases between the subcarriers were varied, and the normalized OSNR versus the phase $\Delta\phi$ for all five subcarriers (Ch1-5) was measured for the three modulation formats (a) ASK, (b) DPSK, and (c) BPSK.

The 3-dB bandwidth of the OBPF, in this case, was around twice the bit rate (20 GHz). As expected, the performance variations of Ch1/Ch5 were less than that of the center subcarrier (Ch3) and Ch2/Ch4, and the performance was optimal when the phase difference between adjacent subchannels was $\pm\pi/2$, where the residual crosstalk from the inner neighbors was orthogonal to the signal. On the other hand, when the signal-crosstalk beating was not mitigated $(\Delta\phi = 0, \pi, 2\pi)$, an additional 3–5 dB OSNR penalty was induced for Ch3.

3.2. Simulations for a Three-Subcarrier CoWDM System

In order to enable direct comparison with the experimental results that will be discussed in Section 4, and to demonstrate the impact of using only two modulators in an odd/even modulated configuration, the simulations from Section 3.1 were performed but in a three-subcarrier DPSK CoWDM system. Here, two different scenarios were used: i) with all optical subcarriers independently modulated (independently modulated configuration) and ii) where only two modulators were used (odd/even modulated configuration), i.e., the outer subcarriers were modulated with the same data. In the simulations with the independently modulated configuration, three optical subcarriers with the same intensity and phase were generated by an optical comb generator and modulated by DPSK data individually. The bandwidth of the modulator was set to be 13 GHz. The simulated data parameters, including the PRBS length and boundary conditions, were the same as Section 3.1. Additional phase shifts (0, $\Delta\phi$, 0) were placed on each subcarrier to investigate the phase influence. At the receiver, the signals were demultiplexed by a 0.3-nm Gaussian-shaped filter, an AMZI with an FSR of 20 GHz and a 20-dB extinction ratio, and a third-order Gaussian-shaped bandwidth-tunable

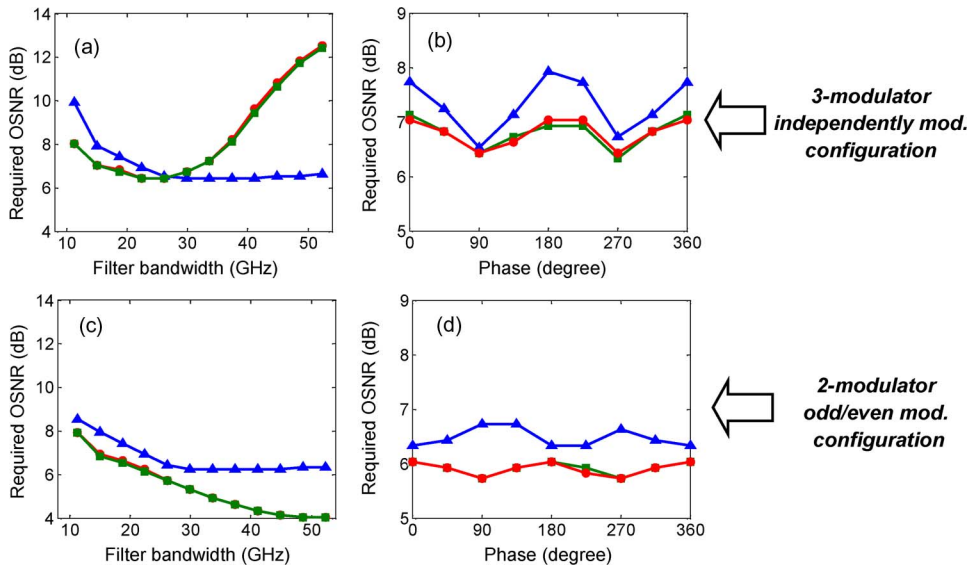

Fig. 7. Three-subcarrier DPSK CoWDM system performance as a function of the OBPF bandwidth [left—(a), (c)] and the phase $\Delta\phi$ [right—(b), (d)] for independently mod. configuration (top) and odd/even mod. configuration (bottom) (Ch1: red circles; Ch2: blue triangles; Ch3: green squares).

optical filter. The received optical power at the receiver was 0 dBm, and a 7-GHz Bessel electrical filter was also deployed at the receiver. The performance for the independently modulated configuration as a function of filter bandwidth is illustrated in Fig. 7(a), where circles, triangles, and squares represent the left (Ch1), center (Ch2), and right (Ch3) subcarriers, respectively.

The optimal bandwidth of the outer (Ch1 and Ch3) subcarriers was 25 GHz, and the overall bandwidth, including the 0.3-nm filter, was around 20 GHz, which is similar to that in the five-subcarrier case. However, in contrast, the optimal filter bandwidth for the center subcarrier was between 30–50 GHz, which is wider than that of the neighboring subcarriers (Left/Right) at optimized phases. This is because only three subcarriers were used, such that no outer-neighbors existed, which would cause penalties as the filter bandwidth increased. Fig. 7(b) shows the required normalized OSNR versus the phase for the independently modulated configuration. The bandwidth of the tunable OBPF was 26 GHz for the outer subcarriers (Left/Right) and 45 GHz for center one. The figure also shows that $\pi/2$ was the optimal phase to achieve the best performance for this configuration, and the performance of the center subcarrier was more dependent on the relative phase. On the other hand, in order to investigate the effect of using the same data patterns for the adjacent neighboring subcarriers on the performance, we also simulate a three-subcarrier CoWDM system with odd/even modulated configuration. In this simulation, three optical subcarriers were separated into even and odd paths by an AMZI disinterleaver, and the relative phase of the center subcarrier was controlled with respect to the outer channels by a phase shift of $\Delta\phi$. The demultiplexing setup was the same as that of the independently modulated configuration. Fig. 7(c) shows that, when compared with Fig. 7(a), the overall performances for all subcarriers were improved by using the odd/even modulated configuration, which we attribute primarily due to the loss of crosstalk from non-identical inner neighbors, as identified in Section 2. Another typical feature of the figure is that the required OSNR decreased below the value for an isolated sub-carrier with the OBPF bandwidth. This is attributed to the fact that both subcarriers carried the same data, and a wider bandwidth increased the signal power instead of crosstalk. Fig. 7(d) depicts the performance versus the phase. The bandwidth of the OBPF was 26 GHz for the outer subcarriers (Left/Right) and 45 GHz for center subcarrier, for a fair comparison with Fig. 7(b). The figure shows that Ch1 and Ch3 exhibited an improved performance and a similar profile as those in Fig. 7(b). However, the profile of Ch1 was somewhat different. Due to a π phase shift, which was introduced between the Left and Right optical subcarriers when they were disinterleaved by the AMZI, and to the same data

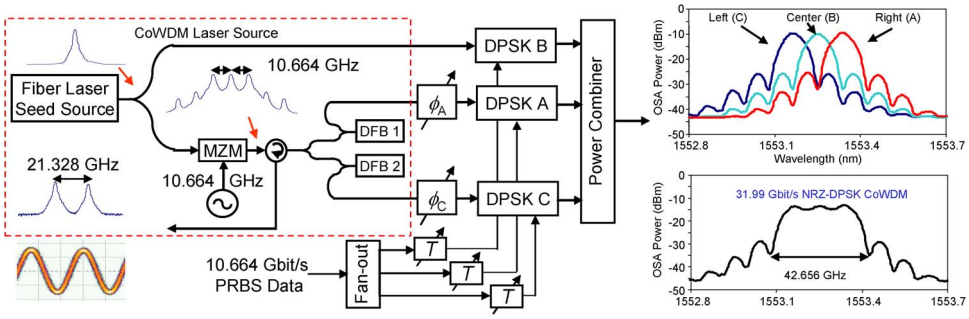

Fig. 8. Experimental setup for independently mod. 32-Gbit/s DPSK CoWDM Tx (left), including beat signal between the three subcarriers (bottom-left). Spectrum of the three individual 10.664-Gb/s DPSK subcarriers (top-right) prior to power combiner, and CoWDM spectrum (bottom-right).

patterns between these two subcarriers, any crosstalk from $D_{j-1,m}$ and $D_{j+1,m}$ to $D_{j,m}$ would be canceled. In this case, the influence from other crosstalk terms, excluding $D_{j\pm1,m}$, which were not included in Section 2, became visible. These terms resulted in an optimized $\Delta\phi$ of 0 and π, instead of $\pi/2$. The contributions of these crosstalk terms were present but were small, with an OSNR fluctuation of less than 0.4 dB.

4. Experiments

In Section 2, it was observed that the use of only two modulators in an odd/even configuration neglects penalties arising from different data symbols on the two nearest interfering channels. This was verified by the numerical simulations in Section 3. To experimentally verify this, independent modulation of a minimum of three subcarriers is required. A general CoWDM schematic is shown in Fig. 4, where a single laser source is used as a seed to a comb generator, whose output is typically followed by an amplifier, in order to maintain an adequate OSNR, and a demultiplexer to separate each subcarrier prior to modulation. An alternative method for subcarrier generation and data encoding is the use of injection locked lasers (CW or tunable) [11]–[13], [22], [23], which enables each laser to be phase locked to one of the selected comb lines, avoiding excess loss of additional components, and providing high extinction ratio and power efficiency. In this section, we present the experimental investigation of a three-subcarrier 32-Gbit/s DPSK CoWDM system in the two configurations used in the simulations in Section 3.2, i.e., using three independent modulators (see Section 4.1) (independently modulated subcarriers), based on injection locked lasers, and, second, using a more traditional scheme of odd/even modulated subcarriers (see Section 4.2) using a standard comb generator. These two experiments show the impact of the additional crosstalk terms that appear when more than two data encoding streams are used. Note that, because, in a practical experimental realization, the different subcarriers actually go through different paths, and unless an integrated device is used, random environment changes will cause each separate path to suffer from random length change, resulting in random phase variations. In order to compensate for the phase variations, a phase-stabilization circuit is required [10], but in this paper, since the temperature was kept fairly stable, the phase adjustments were made manually.

4.1. Independently Modulated 3-Subcarrier DPSK CoWDM System

The experimental setup for the independently modulated three-subcarrier DPSK CoWDM system is shown in Fig. 8 (left). The output of a fiber laser source (centered at 1553.175 nm) was split as follows: 10% was used for the center subcarrier, and the remaining 90% was used to generate a three-line comb signal spaced at 10.664 GHz using a single Mach–Zehnder modulator (MZM). The three-line comb signal then was launched to a circulator and a splitter (all polarization maintaining) in order to injection lock two DFB lasers, corresponding to the left and right spectral lines from the center subcarrier, resulting in left and right subcarriers spaced by 21.328 GHz. The 21.326-GHz beat signal between the left and right subcarriers was observed at the third output of the circulator, as

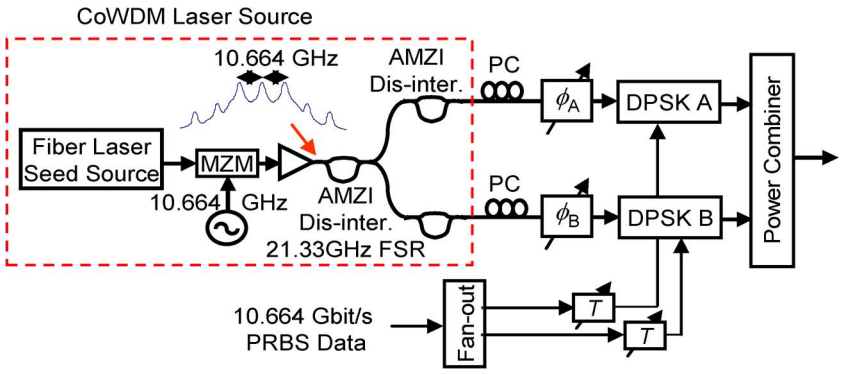

Fig. 9. Experimental setup for 32-Gbit/s DPSK CoWDM in an odd/even modulated configuration.

shown in Fig. 8 (bottom-left), confirming that both lasers were successfully injection locked in frequency and phase. The use of injection locked lasers enables the power of the subcarriers to be equalized, relaxing the power and flatness constraints imposed on the primary comb generator, and improving the OSNR and power efficiency [11], [12]. Each of the three-subcarriers were independently DPSK modulated by a 10.664-Gbit/s electrical data stream with a pseudo random bit sequence (PRBS) length of $2^{31} - 1$. The data streams had a -10-bit and $+7$-bit delays for the left and right subcarriers, respectively. A piezo-electric fiber stretcher was inserted after the output of each injection locked DFB laser in order to adjust the relative phases of the outer subcarriers to the center one. The 3DPSK modulated subcarriers were then combined using a planar waveguide power combiner, resulting in a 32-Gbit/s DPSK CoWDM signal as shown in Fig. 8 (right).

4.2. Odd/Even Modulated Three-Subcarrier DPSK CoWDM System

For comparison with the setup in Section 4.1, the experimental setup from Fig. 8 was manipulated in order to achieve a three-subcarrier DPSK CoWDM system with a conventional odd/even modulated configuration, as shown in Fig. 9.

A three-line comb signal was generated from the same source used in the previous section (fiber laser and MZM). A standard commercial MZM was modulated with less than V_π by a 10.664-GHz clock signal to generate two side-bands, such that any additional harmonics were suppressed by more than 25 dB. The side-bands were separated from the central carrier by the clock frequency (10.664 GHz), and the dc-bias was used to match the amplitude of these side-bands to the central carrier with a flatness of less than 0.5 dB. This signal was amplified and launched to cascaded dis-interleavers based on AMZIs (Kylia), with free spectral range (FSR) of 21.33 GHz, to separate the odd (center) and even (left and right) subcarriers. Cascading the AMZIs increases the extinction ratio from around 21 dB, where coherent crosstalk would degrade the signal to $>$ 40 dB, where such crosstalk may be neglected. The additional loss associated with such cascaded filtering would be avoided by the use of injection locked lasers, as per Section 4.1. Two de-correlated 10.664-Gbit/s electrical data streams (with 26-bit differential delay) and a PRBS length of $2^{31} - 1$ were used to drive the two DPSK modulators to modulate the odd and even subcarriers with different data before optically combining them resulting in a 32-Gbit/s DPSK CoWDM signal. Piezo-electric fiber stretchers were also inserted in the optical paths to adjust the phase between the odd and even subcarriers.

4.3. Receiver

For both transmitter cases, the receiver configuration used is shown in Fig. 10. The pre-amplified scheme used a variable optical attenuator (VOA) to vary the input power to the receiver, followed by a low noise pre-amplifier (EDFA 1). An optical 0.3-nm-bandwidth tunable bandpass filter was used to select the subcarrier under test, followed by an AMZI (Kylia), with an FSR of 21.33 GHz, to suppress the adjacent subcarriers. A second amplifier (EDFA 2) was used to boost the signal power

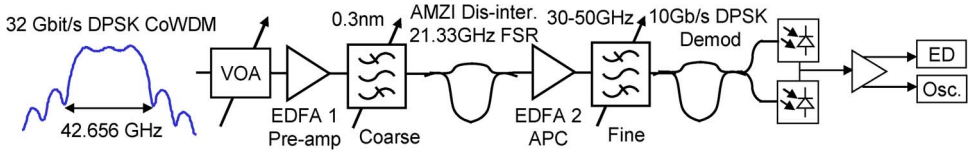

Fig. 10. Experimental setup for a 32-Gbit/s DPSK CoWDM Receiver.

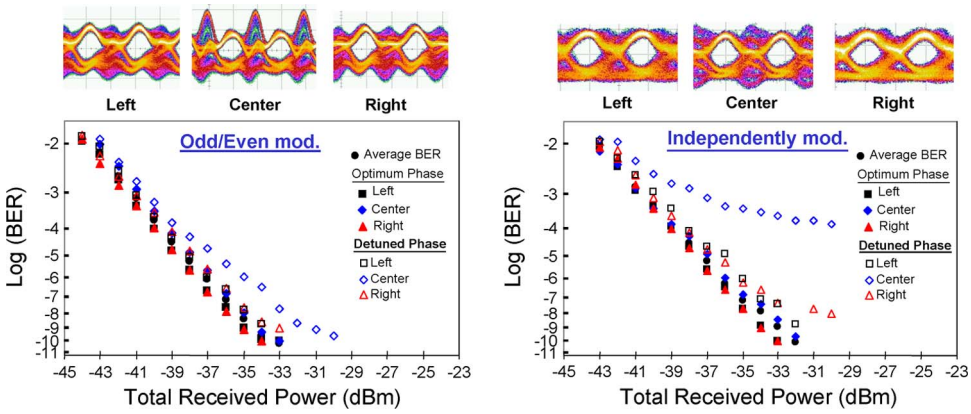

Fig. 11. 32-Gbit/s DPSK CoWDM for optimal and detuned relative phases for odd/even modulated (left) and independently modulated (right) transmitter configurations with corresponding demodulated eye diagrams (top).

to the remaining receiver, comprising a bandwidth adjustable filter, which was optimized for each received subcarrier (50 GHz for the center and 30 GHz for the outer subcarriers), and a DPSK demodulator (1-bit delay AMZI). The demodulated signal was detected using a balanced photodiode and amplified using a limiting differential amplifier and then launched to the error detector (ED) and high speed oscilloscope (Osc.).

4.4. Experimental Results

The performance of both CoWDM transmitter implementations was evaluated by measuring the BER waterfall curves of the three received CoWDM subcarriers. The results shown in Fig. 11 take into account adjustments of the relative phases for optimal performance (lowest BER) and detuning them for a degraded BER.

The average receiver sensitivity (total received power to achieve an average BER of 10^{-9} for the 3-subcarriers was -33.2 dBm and -34.5 dBm for the independently modulated and odd/even modulated configurations, respectively, showing a clear 1.3-dB improvement when odd/even subcarriers were used. When the relative phases are detuned, there is a negligible penalty for the outer subcarriers, with a larger deterioration for the center one. Moreover, for the independently modulated configuration, a BER floor at around 10^{-4} is evident for the center subcarrier. This error floor, at a detuned phase, and the enhanced receiver sensitivity, at the optimum phase, are due to the fact that the center subcarrier is more affected from the interference of the neighboring subcarriers carrying different data patterns and, in particular, when the neighboring subcarriers carry inverted data symbols. This observation also agrees with the simulation results shown in Fig. 7(b) and (d). Such interference could be reduced, or even eliminated, by using an improved filter that is closer to a matched or ideal filter at the receiver. The demodulated eye diagrams for the subcarriers for both configurations are also shown in Fig. 11 (top). It should be noted that, for the odd/even modulated case, a strong beating signal is observed for the center subcarrier as both neighbor subcarriers carry the same data patterns, which is not the case for the center channel in

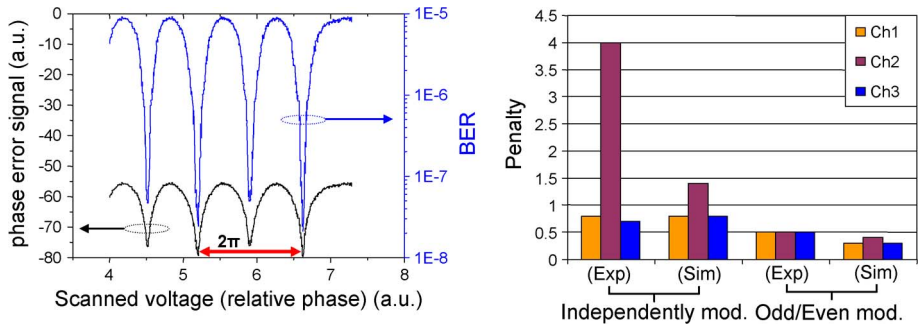

Fig. 12. (Left) BER for the center subcarrier against the relative phase in an odd/even mod. configuration. (Right) Ratio between best and worst phases performance for numerically simulated (Sim) and experimentally implemented (Exp) three-subcarrier 10-GBd DPSK CoWDM system.

the independently modulated configuration. The BER for the center subcarrier, in an odd/even modulated configuration, was also measured when varying the relative phase of the outer subcarriers, as shown in Fig. 12 (left). It clearly shows the periodicity with phase ϕ, as predicted analytically and numerically (Figs. 3 and 7, respectively). Fig. 12 (right) shows a comparison in terms of numerically simulated received OSNR penalty (for a three-subcarrier 30 Gbit/s DPSK system) and experimentally observed received power penalty (for a three-subcarrier 32 Gbit/s DPSK system) between the best and worse phase performances required to obtain a BER of 5×10^{-4} for both independently modulated and odd/even modulated configurations. In all cases, it is clearly shown that the center subcarrier will always be further deteriorated, as it has the impact of both outer subcarriers. As predicted, the odd/even modulated configuration gives lower penalties, as some of the analytical terms are null. The difference in the results obtained numerically and experimentally could be due to non-ideal components used in the experimental setup.

5. Conclusion

We have presented analytical and numerical analyses which assess the impact of the relative phase relationship between subcarriers on CoWDM systems, using direct detection for ASK and differential/coherent detection for BPSK. These analyses were also verified experimentally using differential detection for DPSK signals. We have further demonstrated that the commonly used odd/even configuration may under-estimate the average receiver sensitivity penalty by 1.3 dB when compared with practical implementations using an independently modulated configuration. However, in all cases, by controlling the relative phases between the sub-carriers, the receiver sensitivity could be improved, avoiding large penalties and possible error floors. We conclude that low-cost optical receiver filters can therefore be used without sacrificing the performance, hence avoiding extra receiver complexity, and enabling a practical implementation of CoWDM.

References

[1] R.E Mosier and R.G Clabaugh, "Kineplex, a bandwidth-efficient binary transmission system," *AIEE Trans.*, vol. 76, pp. 723–728, Jan. 1958.

[2] H. Sanjoh, E. Yamada, and Y. Yoshikuni, "Optical orthogonal frequency division multiplexing using frequency/time domain filtering for high spectral efficiency up to 1 bit/s/Hz," in *Proc. OFC*, 2002, pp. 401–402, ThD1.

[3] K. Yonenaga, F. Inuzuka, S. Yamamoto, H. Takara, B. Kozicki, T. Yoshimatsu, A. Takada, and M. Jinno, "Bit-rate-flexible all-optical OFDM transceiver using variable multi-carrier source and DQPSK/DPSK mixed multiplexing," in *Proc. OFC*, 2009, pp. 1–3, OWM1.

[4] A. Sano, H. Masuda, E. Yoshida, T. Kobayashi, E. Yamada, Y. Miyamoto, F. Inuzuka, Y. Hibino, Y. Takatori, K. Hagimoto, T. Yamada, and Y. Sakamaki, "30 $\times$ 100 Gb/s all-optical OFDM transmission over 1300 km SMF with 10 ROADM nodes," in *Proc. ECOC*, 2007, pp. 1–2, PD1.7.

[5] S. Chandrasekhar, X. Liu, B. Zhu, and D. W. Peckham, "Transmission of a 1.2-Tb/s 24-carrier no-guard-interval coherent OFDM superchannel over 7200-km of ultra-large-area fiber," in *Proc. ECOC*, 2009, pp. 1–2, PD2.6.

[6] D. Hillerkuss, M. Winter, M. Teschke, A. Marculescu, J. Li, G. Sigurdsson, K. Worms, S. Ben Ezra, N. Narkiss, W. Freude, and J. Leuthold, "Simple all-optical FFT scheme enabling Tbit/s real-time signal processing," *Opt. Express*, vol. 18, no. 9, pp. 9324–9340, Apr. 2010.
[7] K. Takiguchi, M. Oguma, H. Takahashi, and A. Mori, "Integrated-optic eight-channel OFDM demultiplexer and its demonstration with 160 Gb/s signal reception," *Electron. Lett.*, vol. 46, no. 8, pp. 575–576, Apr. 2010.
[8] H. Chen, M. Chen, and S. Xie, "All-optical sampling orthogonal frequency-division multiplexing scheme for high-speed transmission system," *J. Lightw. Technol.*, vol. 27, no. 21, pp. 4848–4854, Nov. 2009.
[9] A. D. Ellis and F. C. G. Gunning, "Spectral density enhancement using coherent WDM," *IEEE Photon. Technol. Lett.*, vol. 17, no. 2, pp. 504–506, Feb. 2005.
[10] F. C. G. Gunning, T. Healy, X. Yang, and A. D. Ellis, "0.6 Tbit/s capacity and 2 bit/s/Hz spectral efficiency at 42.6 Gsymbol/s using a single DFB laser with NRZ coherent WDM and polarisation multiplexing," in *Proc. CLEO-Eur.*, 2007, p. 1CI8-5-FRI.
[11] S. K. Ibrahim, A. D. Ellis, F. C. G. Gunning, J. Zhao, P. Frascella, and F. H. Peters, "Practical implementation of coherent WDM," in *Proc. IEEE Photon. Soc. Meet.*, 2009, pp. 715–716, Invited paper ThM1.
[12] S. K. Ibrahim, A. D. Ellis, F. C. G. Gunning, and F. H. Peters, "Demonstration of CoWDM using a DPSK modulator array with injection-locked lasers," *Electron. Lett.*, vol. 46, no. 2, pp. 150–152, Jan. 2010.
[13] S. K. Ibrahim, F. C. G. Gunning, and A. D. Ellis, "Performance evaluation and comparison of DPSK CoWDM systems based on odd/even and array configurations," in *Proc. CLEO*, 2010, pp. 1–3, CThC3.
[14] A. J Lowery, L. Du, and J. Armstrong, "Orthogonal frequency division multiplexing for adaptive dispersion compensation in long haul WDM systems," in *Proc. NFOEC*, 2006, pp. 1–3, PDP39.
[15] B. J. C. Schmidt, A. James Lowery, and J. Armstrong, "Experimental demonstrations of 20 Gb/s direct-detection optical OFDM and 12 Gb/s with a colorless transmitter," in *Proc. OFC*, 2007, pp. 1–3, PDP18.
[16] A. Sano, E. Yamada, H. Masuda, E. Yamazaki, T. Kobayashi, E. Yoshida, Y. Miyamoto, R. Kudo, K. Ishihara, and Y. Takatori, "No-guard-interval coherent optical OFDM for 100-Gb/s long-haul WDM transmission," *J. Lightw. Technol.*, vol. 27, no. 16, pp. 3705–3713, Aug. 2009.
[17] W. Shieh, H. Bao, and Y. Tang, "Coherent optical OFDM: Theory and design," *Opt. Express*, vol. 16, no. 2, pp. 841–859, Jan. 2008.
[18] W. Shieh, Q. Yang, and Y. Ma, "107 Gb/s coherent optical OFDM transmission over 1000-km SSMF fiber using orthogonal band multiplexing," *Opt. Express*, vol. 16, no. 9, p. 6378, Apr. 2008.
[19] S. L. Jansen, I. Morita, T. C. W. Schenk, and H. Tanaka, "121.9-Gb/s PDM-OFDM transmission with 2-b/s/Hz spectral efficiency over 1000 km of SSMF," *J. Lightw. Technol.*, vol. 27, no. 3, p. 177, Feb. 2009.
[20] J. Zhao and A. D. Ellis, "Electronic signal processing for crosstalk- and ISI-free operation in all-optical OFDM," in *Proc. ECOC*, 2010, pp. 1–3, Paper Tu.4.A.7.
[21] G. Gavioli, E. Torrengo, G. Bosco, A. Carena, V. Curri, V. Miot, P. Poggiolini, M. Belmonte, F. Forghieri, C. Muzio, S. Piciaccia, A. Brinciotti, A. La Porta, C. Lezzi, S. Savory, and S. Abrate, "Investigation of the impact of ultra-narrow carrier spacing on the transmission of a 10-carrier 1 Tb/s superchannel," in *Proc. OFC*, 2010, pp. 1–3, OThD3.
[22] S. K. Mondal, B. Roycroft, P. Lambkin, F. Peters, B. Corbett, P. Townsend, and A. Ellis, "A multiwavelength low-power wavelength-locked slotted Fabry–Pérot laser source for WDM applications," *IEEE Photon. Technol. Lett.*, vol. 19, no. 10, p. 744, May 2007.
[23] B. Cai, D. Wake, and A. J. Seeds, "Microwave frequency synthesis using injection locked laser comb line selection," in *Proc. IEEE LEOS Summer Top. Meet. RF Optoelectron.*, 1995, pp. 13–14, WD213–14.